J. Fluid Mech. (1995), *vol.* 284, *pp.* 23–41

Bifurcation for flow past a cylinder between parallel planes

By J.-H. CHEN,[1] W. G. PRITCHARD[2] AND S. J. TAVENER[2]

[1] Department of Naval Architecture, National Taiwan Ocean University, 2 Pei-Ning Rd, Keelung 202, Taiwan, ROC

[2] Department of Mathematics, Penn State University, University Park, PA 16802, USA

(Received 7 March 1994 and in revised form 13 July 1994)

Numerical experiments are described to ascertain how the steady flow past a circular cylinder loses stability as the Reynolds number is increased. A novel feature of the present study is that the cylinder is confined between parallel planes, allowing a more definitive specification of the flow, both experimentally and computationally, than is possible for the unbounded case. Since the structure of the bifurcation is unclear from the extant literature, with the experimental and computational evidence not in good agreement, a critical appraisal of both sets of evidence is presented.

A study has been made of the formation of the steady vortex pair behind the cylinder, and it has been determined that the first appearance of the vortices is not associated with a bifurcation of the full dynamical problem but instead it is probably associated with a bifurcation of a restricted kinematical problem.

A set of numerical experiments has been made in which the steady flow past the cylinder was perturbed slightly and the ensuing time-dependent motions were computed. These experiments revealed that, for a given blockage ratio, the perturbation would die away at small Reynolds numbers but that, above a critical Reynolds number, the disturbance would be amplified and the flow would eventually settle down to a new state comprising a time-periodic motion.

Experiments were also carried out to determine the bifurcation point numerically by considering an eigenvalue problem based on a linearization about the computed steady flow past the cylinder. The calculations showed that stability is lost through a symmetry-breaking Hopf bifurcation and that, for a given blockage ratio, the critical Reynolds number was in very good agreement with that estimated from the time-dependent computations.

1. Introduction

The flow generated by a cylinder or sphere moving at a steady speed through a fluid provides one of the classic problems of fluid mechanics. In particular, the way in which the steady flow seen at small speeds loses its stability has always been an issue of fascination, with the experimental evidence strongly suggesting that stability is exchanged for a time-periodic motion at a Reynolds number of about 35 in two dimensions and in the range of 120 to 190 for flow past a sphere. Here the Reynolds number R is defined in terms of the diameter of the body. Interestingly, the experimental observations do not give a clear picture of the nature of the bifurcation in either the two- or the three-dimensional case, as illustrated by the following commentary from Batchelor's (1967, p. 260) text, talking about flow past a cylinder: 'At a value of R between 30 and 40, the steady flow appears to become unstable to

small disturbances;... In the present case, the instability first affects the wake, at some distance downstream from the cylinder, and gives rise to a slow oscillation of the wake, approximately sinusoidal in both time and stream-wise distance, with an amplitude which increases with distance downstream.... As R increases, beyond the critical value at which instability first appears, the oscillation in the wake moves closer to the cylinder and, when R is near 60, begins to affect the two standing eddies immediately behind the cylinder.' It is apparent from this commentary that the experimental situation is a rather difficult one to control accurately and that the interpretation of the observations could involve several subtleties. Moreover, recent numerical experiments in two dimensions have not particularly helped clarify the situation. For example, Jackson (1987) estimated the bifurcation point, for a special flow configuration, to be at a Reynolds number of approximately 46.2, well in excess of the experimental values, though his calculations did show that the exchange of stability occurs through a Hopf bifurcation to time-periodic motions.

There are, however, several obstacles to making close comparisons between experiment and theory for exterior flows, most of which derive from the desire to simulate the flow in a domain unbounded in all directions, which conditions cannot obtain experimentally anyway. Simulation of the pure exterior flow problem poses considerable computational difficulties, principally because there are only partial estimates for the decay of solutions of the Navier–Stokes equations at large distances. Accordingly, there is no way of knowing how to truncate the flow domain for computational purposes so as to provide a provable approximation to the flow in the unbounded domain. For example, Jackson (1987) made his computations in a rectangular domain of height 10 units and length 20 units relative to the diameter of the cylinder. On the inlet boundary he imposed Dirichlet data on the velocity $\boldsymbol{u}$ (with components (u, v) in the respective (x, y) directions) such that $\boldsymbol{u} = (1, 0)$ at $x = -5$. On the horizontal boundaries of the box, at $y = \pm 5$, he set $\boldsymbol{u} = (1, 0)$ and, on the outlet boundary, he set $p + \partial u/\partial x = 0$ and $\partial v/\partial x = 0$. Similar kinds of boundary conditions have been used by several other authors in related contexts and though they may well provide some kind of approximation to the exterior flow problem it is not clear, especially with regard to the imposition of the downstream conditions, precisely how they relate to the full problem.

For these reasons we have taken a different view of the situation and decided to consider a flow problem that can be accurately simulated, both experimentally and computationally, but which preserves the essential features of the aforementioned exterior flows. To do this we have relaxed the constraint that the flow be unbounded in all directions, and have placed the body between plane parallel walls which may, however, be considered to be unbounded in the direction parallel to the walls. In three dimensions, our approach would be to place the body within a cylindrical tube.

The theoretical situation for flows in certain classes of pipes and channels is well established (see Amick 1977, 1978, and Amick & Fraenkel 1980) in that it is possible to establish the existence of a solution to the Navier–Stokes equation for such flows over a substantial range of Reynolds numbers. In the event that the channel or pipe approaches a uniform width far upstream and downstream, Amick (1978) showed that the velocity fields approach the appropriate Poiseuille distribution and that the rate of approach is exponential, at least when the Reynolds number is not too large. The exponentially fast approach upstream and downstream of such flows to their asymptotic states means that, by introducing and removing the fluid through sufficiently long uniform regions, it is possible to obtain a very close approximation to the flow in the unbounded domain by considering a flow in a bounded domain. In other

words, the numerical calculations to be described are, in principle, amenable to empirical testing, limited only by the accuracy with which the experiment is carried out. These principles are at the heart of the design of the present numerical experiments, and also of some empirical measurements concerning flow past a sphere described briefly in Pritchard (1983).

The main purpose of this paper is to make some firm predictions concerning the way in which the steady flow past a cylinder at small Reynolds numbers loses stability as the Reynolds number is increased. The predictions made here could be subject to direct experimental verification and, moreover, should shed light on the corresponding flow problem in the unbounded domain. We shall describe numerical results obtained using four different numerical schemes, providing internal consistency checks on our computations, and enabling us to examine different properties of the flow field. Initially we shall describe some results concerning the properties of the steady vortex pair attached to the rear of the cylinder and an estimate of the Reynolds number at which they first appear as the flow rate is increased. The results of such a study are quite useful in that they allow us to assess the properties of the numerical procedures as well as providing a basis of comparison of computed flows between parallel planes with experimental results obtained in essentially unbounded domains. Then we shall describe some apparently periodic solutions to the Dirichlet problem for the Navier–Stokes equation posed in a channel of specified length. By examining carefully the properties of these flows as a function of Reynolds number we have been able to make an estimate of the critical Reynolds number above which such flows are possible. Finally we shall present the results of some eigenvalue calculations used to provide a more definitive estimate of the bifurcation point, the results of which are in good agreement with the aforementioned time-dependent studies. The ENTWIFE code used for the bifurcation studies was also used, in an earlier version, by Jackson in his 1987 studies. Thus, we have recomputed the problem considered by Jackson, as a point of reference, and to check the importance of the length and height of the domain to the computed bifurcation point.

2. Survey of experimental results

There have been many experiments concerning the flow past a circular cylinder at small Reynolds numbers, including those by Taneda (1956*a*), Tritton (1959), Nishioka & Sato (1974), Coutanceau & Bouard (1977*a*, *b*) and Gerrard (1978).†

Taneda's (1956*a*) experiments were made in a water tank through which a cylinder was towed. Measurements were made of the length of the steady wake behind the cylinder as a function of the Reynolds number R and of the wavelength of the oscillations in the wake at Reynolds numbers above that at which the flow became unsteady. The tank had a length of 1 m and cross-section 200×300 mm, and the diameters of his cylinders ranged between 6.00 and 1.02 mm, and their lengths were such that the aspect ratios ranged between 50:1 and 176:1 respectively. For the largest cylinder the walls of the tank were at a distance of 16.5 diameters and for the smallest cylinder they were at 98 diameters. From the experiments it was estimated that the steady vortex pair first appeared behind the cylinder at a Reynolds number of

† One of the referees suggested referring to a paper by Provansal, Mathis & Boyer (1987) who made measurements of the critical Reynolds number in a wind tunnel. Unfortunately the motions had a significant three-dimensional component with extrapolation being needed to an infinite aspect ratio from values of 10.0, 12.5 and 16.7, and so the critical value for two-dimensional flows must have a large subjective component to it.

approximately 5. These became more and more elongated as R was increased until R reached the value of about 45. However, at $R \approx 30$, small sinusoidal oscillations were observed in the wake some distance downstream from the vortices. For values of R exceeding 35 Taneda reported that 'Tiny irregular gathers appear in the boundary of the twin-vortices, move downstream along the boundary-line till they reach the rear end of the twin-vortices, tremble for a short time and are died away.... At Reynolds numbers above 45 the gathers of the twin-vortices are elongated along the trail, shed alternately from each of the twin-vortices and pass downstream, where they arrange themselves in a configuration corresponding to that of a Kármán vortex street'.

In the experiments of Coutanceau & Bouard (1977*a*, *b*) the flow generated by a cylindrical rod rising broadside at constant speed in a cylindrical tank of large diameter (420 mm diameter × 1 m in height) was observed. The tank was filled with an oil having a kinematic viscosity of approximately thirty times that of water. The cylindrical rods used in the experiments had diameters 10.1, 29.4 and 50.4 mm. Careful measurements were made of the properties of the attached vortices immediately behind the cylindrical rod, including their development in time from the sudden initiation of the motion of the rod. Coutanceau & Bouard concentrated their attention mainly on the attached vortex pair immediately behind the cylinder and estimated that the vortex pair would first appear, for a rod in an unbounded flow, when the Reynolds number is increased above a value of about 4.5, in good agreement with the measurements of Taneda (1956*a*). As the Reynolds number was further increased they estimated that 'the upper limit of wake stability' ('critical Reynolds number') was approximately 39.5 in the case of the 29.4 mm rod. Interestingly, they characterized the critical Reynolds number by a loss in symmetry of the vortex pair: '... the wake boundary begins to warp towards its rear end and the distances between each of the cores and the rear stagnation point become different'.

The experiments of Gerrard (1978) were similar in concept to those of Taneda (1956*a*). They were carried out in a towing tank of length 4 m, width 750 mm and depth 460 mm, which was filled with water. The cylinders used in these experiments had diameters 25.4, 12.65, 10.3, 6.3 and 4.7 mm. They were mounted on a towing carriage with their axes vertical and moved at steady speed along the centre of the tank. In trying to estimate the critical Reynolds number at which time-dependent flows first appeared, Gerrard made the following comment: 'In view of the sensitivity to disturbances any determination of the Reynolds number for what might be called the onset of oscillations is likely to be inaccurate and a function of the particular experimental arrangement'. Gerrard estimated the critical Reynolds number at which unsteady flows first appear to be about 34, and at $R = 37.8$ he describes the flow in the vortex pair immediately behind the cylinder to be unsteady, but there was no indication of the formation of a vortex street under these conditions.

It is thus seen from the above discussion that, while the various experimenters are all in general agreement with each other, the details of the wake region near the critical Reynolds number for the onset of unsteady flows would appear to be sensitively different from experiment to experiment (cf. the comments of Gerrard). In particular, Coutanceau & Bouard point to the formation of a steady non-symmetrical vortex pair, whereas Gerrard found this region to be unsteady. One issue about which all authors appear to agree is that the critical Reynolds number for the formation of unsteady flows is in the mid to upper 30s, which values would appear to be significantly different from the 46.2 predicted by Jackson (1987). It is evident that the issues associated with this bifurcation are delicate enough, even to the point of questioning whether, in an unbounded domain, the exchange of stability occurs via a Hopf bifurcation or via a

symmetry-breaking bifurcation to a steady flow, with a subsequent secondary bifurcation to a Hopf flow. The latter proposition would not be out of keeping with the description given by Coutanceau & Bouard (1977*a*). Also it has been found by Fearn, Mullin & Cliffe (1990) for the sudden expansion between parallel plates, that the bifurcation is to a steady symmetry-breaking flow.

The bifurcation structure is, if anything, less clear for the analogous situation of flow past a sphere. Taneda's (1956*b*) experiments, made by towing a sphere, indicated oscillations in the wake region at Reynolds numbers exceeding 130. Then, in 1976, Nakamura made observations of the wake behind a sphere steadily falling in water and found the wake to be symmetrical and steady at Reynolds numbers up to values of approximately 190, at which point the wake became distinctly non-symmetrical but the flow remained steady. Supporting the conclusions of Nakamura (1976), Wu & Faeth (1993) observed the wake of a towed sphere to be symmetrical and steady for Reynolds numbers less than 200, and to be steady but asymmetrical for Reynolds numbers between 200 and 280. The results of numerical studies made by Kim & Pearlstein (1990), using a modal decomposition to affect a linear stability analysis, indicated a symmetry-breaking bifurcation of Hopf type at a Reynolds number of approximately 175.1. By contrast, some recent calculations by Natarajan & Acrivos (1993), using similar methods, indicate that the first instability has the same azimuthal wavenumber as that predicted by Kim & Pearlstein but that the bifurcation is to a non-symmetrical steady flow, occurring at Reynolds number 210.

3. The mathematical problem to be solved

The mathematical problem under consideration is that of finding the velocity, $\boldsymbol{u}(\boldsymbol{x}, t) = (u, v)$, and the pressure, $p(\boldsymbol{x}, t)$, as functions of position $\boldsymbol{x} = (x, y)$ and time t, which satisfy the incompressible Navier–Stokes equations

$$R\left(\frac{\partial \boldsymbol{u}}{\partial t} + \boldsymbol{u}\cdot\nabla\boldsymbol{u}\right) = -\nabla p + \Delta\boldsymbol{u}, \tag{1}$$

and

$$\nabla\cdot\boldsymbol{u} = 0. \tag{2}$$

Equations (1) and (2) are to be solved on a domain $\Omega \subset \mathbb{R}^2$, a typical example of which is sketched in figure 1. A circular cylinder, of diameter d, is centrally located between two parallel planes separated by unit distance. The domain has length L and the cylinder is located a distance L_1 from the upstream boundary, through which fluid is introduced to the flow domain.

Two different kinds of problem will be considered. The first, which represents flow between solid plane boundaries, will form the basis for the bulk of our calculations. For this class of flows we shall specify Dirichlet data (namely a parabolic horizontal velocity profile and zero vertical velocity) on the upstream boundary AB. On the horizontal boundaries AD and BC, and on the boundary of the cylinder we shall impose no-slip Dirichlet data, and on the downstream boundary either Dirichlet or Neumann-type conditions will obtain. The second class of flow problems to be considered are intimately related to the problem considered by Jackson (1987) and outlined briefly in §1. These problems are meant to simulate flow in an unbounded domain and will be used here mainly as a point of comparison with Jackson's study.

Let us suppose that the flux of fluid across the upstream boundary is Q and let the fluid viscosity be ν. Then the non-dimensionalization pertaining to (1) has the Reynolds number $R = Q/\nu$, all lengths are scaled with respect to the distance between the plane

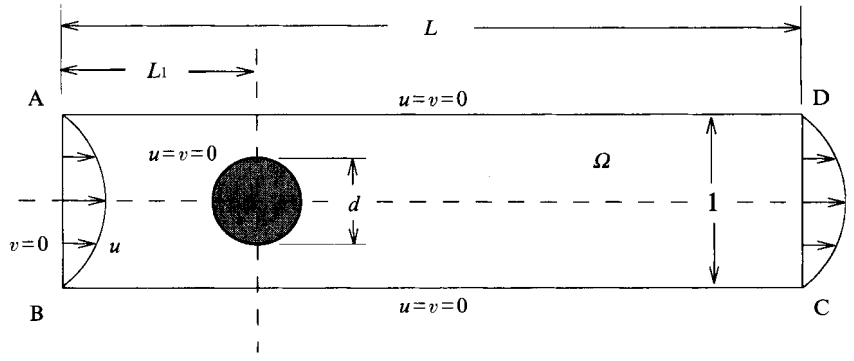

FIGURE 1. Schematic representation of the computational domain.

walls and time is scaled by Q^{-1}. In some circumstances it will also be convenient to quote a Reynolds number, $R_d = U_d d/\nu$, based on the cylinder diameter, where

$$U_d = \frac{1}{d}\int_{-d/2}^{d/2} u(y)\,\mathrm{d}y.$$

Here u is the horizontal component of the velocity field specified on the upstream boundary. The Reynolds number R_d is useful when making comparisons with experimental results obtained on what are effectively unbounded domains.

In most of the calculations to be presented we shall be interested in solutions to and bifurcation analyses for the steady problem defined by (1) and (2), but in §6 the results of some time-dependent calculations will be reported.

4. Numerical methods

We wish to solve the Navier–Stokes equations (1) and (2) with Dirichlet boundary conditions $\boldsymbol{u}(\boldsymbol{x}) = \boldsymbol{g}(\boldsymbol{x})$ imposed on part of the boundary $\partial\Omega_d$ and Neumann conditions on the remainder of the boundary $\partial\Omega_n$. (We assume that the boundary $\partial\Omega$ is partitioned into two disjoint sets $\partial\Omega_d$ and $\partial\Omega_n$ whose union comprises the entire boundary.)

The usual variational formulation for the *steady* version of the Navier–Stokes equations is derived by taking the dot-product of equation (1) with an appropriate vector function $\boldsymbol{v}$, and the scalar-product of (2) with a suitable scalar function q, integrating the equations over the domain Ω and integrating by parts where appropriate. The resulting equations are

$$a(\boldsymbol{u},\boldsymbol{v}) + b(\boldsymbol{v},p) + c(\boldsymbol{u},\boldsymbol{u},\boldsymbol{v}) = 0, \tag{3}$$

and

$$b(\boldsymbol{u},q) = 0, \tag{4}$$

where the various forms are defined by

$$a(\boldsymbol{u},\boldsymbol{v}) := \int_\Omega \nabla\boldsymbol{u} : \nabla\boldsymbol{v}\,\mathrm{d}\boldsymbol{x} = \int_\Omega \sum_{i,j=1}^{2} u_{i,j} v_{i,j}, \tag{5}$$

$$b(\boldsymbol{v},q) := -\int_\Omega (\nabla\cdot\boldsymbol{v})\,q\,\mathrm{d}\boldsymbol{x} = -\int_\Omega \sum_{i=1}^{2} v_{i,i}\,q, \tag{6}$$

$$c(\boldsymbol{u},\boldsymbol{v},\boldsymbol{w}) := R\int_\Omega (\boldsymbol{u}\cdot\nabla)\,\boldsymbol{v}\cdot\boldsymbol{w}\,\mathrm{d}\boldsymbol{x} = R\int_\Omega \sum_{i,j=1}^{2} u_i v_{j,i} w_j. \tag{7}$$

An appropriate choice for the functions v and q is that they belong to the spaces V and Π, where

$$V := \{v \in \boldsymbol{W}_2^1(\Omega): v = \mathbf{0} \quad \text{on} \quad \partial\Omega_d\}, \tag{8}$$

and

$$\Pi := \left\{q \in L^2(\Omega): \int_\Omega q(\boldsymbol{x})\,\mathrm{d}\boldsymbol{x} = 0\right\}. \tag{9}$$

Here L^2 and $\boldsymbol{W}_2^1$ respectively denote the usual Sobolev spaces of square-integrable functions and of functions whose first derivatives are square-integrable. With the above definitions and the space

$$V_g := \{v \in \boldsymbol{W}_2^1(\Omega): v = g \quad \text{on} \quad \partial\Omega_d\}, \tag{10}$$

it can be shown (e.g. see Gunzburger 1989) that $\boldsymbol{u}$ and p can be characterized as solving the following variational problem.

Find $\boldsymbol{u} \in V_g$ and $p \in \Pi$ with the property that (3) and (4) hold for all $v \in V$ and for all $q \in \Pi$.

Discrete versions of (3) and (4) can be realized by appropriate choices of discrete counterparts of the spaces V, V_g and Π defined in (8), (10) and (9). A number of different methods have been used in the present study. They were as follows.

(i) The so-called Taylor–Hood method (see Taylor & Hood 1973), based on a triangulation of the domain and using C^0, piecewise quadratic functions, to approximate the velocity space, and C^0, piecewise linear functions to approximate the pressure space. The method was used within the code FIDAP (see Engelman 1982). Some convergence studies of this implementation are reported in Pritchard, Scott & Tavener (1992).

(ii) The $P_2^+ - P_1$ method of Crouzeix & Raviart (see Crouzeix & Raviart 1973). This method, also based on a triangulation of the domain, uses the same approximating functions as for the Taylor–Hood method, but the velocity space is augmented by a 'bubble' function on each triangle, a polynomial of degree three which vanishes along the triangle sides. The method is implemented in FIDAP.

(iii) The $P_1 - P_0$ method of Crouzeix & Raviart (see Crouzeix & Raviart 1973). This method is based on a triangulation of the domain and uses piecewise linear functions, continuous at triangle midpoints only, to approximate the velocity space and discontinuous piecewise constant functions to approximate the pressure space. This method was implemented within an in-house code, details of which may be found in Lodge, Pritchard & Scott (1991).

(iv) A method developed by Bercovier & Engelman (1979), based on a quadrilateralization of the domain. The method uses C^0, piecewise quadratic functions to approximate the velocity space and discontinuous piecewise linear functions to approximate the pressure space. This method was used for the stability and bifurcation computations, and is implemented in the code ENTWIFE (see Winters 1985).

Note that methods (i), (ii) and (iv) use isoparametric elements. Penalty methods were employed to enforce the divergence condition in (i) and (ii); in (iii) the velocity space was constructed to be divergence free on each triangle; (iv) is solved via a mixed method.

For the time-dependent calculations to be reported in §6 the Taylor–Hood method (i) was used for the spatial discretization and the time-stepping was effected via a Crank–Nicholson method.

In order to carry out the eigenvalue calculations to be described in §7 we assume

$(\boldsymbol{u}_0, p_0)$ to be a steady solution of (3) and (4), and consider perturbations about this solution of the form

$$(\boldsymbol{u}_0, p_0) + \epsilon(\boldsymbol{u}_1 \exp(-\gamma t), p_1 \exp(-\gamma t)), \tag{11}$$

where $0 < \epsilon \ll 1, \boldsymbol{u}_1 \in V, p_1 \in \Pi$, and γ is a complex constant. Substituting into (3) and (4) and retaining terms up to order ϵ, the equations governing the perturbation are

$$R[-\gamma \boldsymbol{u}_1 + (\boldsymbol{u}_0 \cdot \nabla)\boldsymbol{u}_1 + (\boldsymbol{u}_1 \cdot \nabla)\boldsymbol{u}_0] = -\nabla p_1 + \Delta \boldsymbol{u}_1 \tag{12}$$

and

$$\nabla \cdot \boldsymbol{u}_1 = 0. \tag{13}$$

A weak formulation of (12) and (13) is developed in the same manner as for (3) and (4), resulting in the equations

$$-\gamma(\boldsymbol{u}_1, \boldsymbol{v}) + a(\boldsymbol{u}_1, \boldsymbol{v}) + b(\boldsymbol{v}, p_1) + c(\boldsymbol{u}_0, \boldsymbol{u}_1, \boldsymbol{v}) + c(\boldsymbol{u}_1, \boldsymbol{u}_0, \boldsymbol{v}) = 0, \tag{14}$$

and

$$b(\boldsymbol{u}_1, q) = 0, \tag{15}$$

where

$$(\boldsymbol{u}, \boldsymbol{v}) := R \int_\Omega \boldsymbol{u} \cdot \boldsymbol{v} \, \mathrm{d}\boldsymbol{x} = R \int_\Omega \sum_{i=1}^{2} u_i v_i.$$

Using mixed finite elements to solve (14) and (15) results in a generalized eigenvalue problem. Let $\boldsymbol{w} \in \mathbb{R}^k$ be the vector of nodal freedoms defining the velocity perturbation $\boldsymbol{u}_1$ and let $\boldsymbol{p} \in \mathbb{R}^l$ be the vector of freedoms defining the pressure perturbation p_1. The discretized form of (14) and (15) is then

$$\begin{pmatrix} \boldsymbol{K} & \boldsymbol{C} \\ \boldsymbol{C}^T & 0 \end{pmatrix} \begin{pmatrix} \boldsymbol{w} \\ \boldsymbol{p} \end{pmatrix} = \gamma \begin{pmatrix} \boldsymbol{M} & 0 \\ 0 & 0 \end{pmatrix} \begin{pmatrix} \boldsymbol{w} \\ \boldsymbol{p} \end{pmatrix}, \tag{16}$$

where $\boldsymbol{K}$ is a $(k \times k)$ sparse non-symmetric matrix, $\boldsymbol{C}$ is a $(k \times l)$ matrix of rank l, and $\boldsymbol{M}$ is a $(k \times k)$ symmetric matrix. The eigenvalue problem (16) is real but non-symmetric, hence eigenvalues will be either real or occur in complex-conjugate pairs. Accordingly, there is a need to locate the eigenvalue(s) with *smallest real part* for any given flow rate. In the present calculations this has been achieved by the use of a mapping (a Cayley transform) of the complex plane and then using subspace-iteration techniques to determine the most dangerous eigenvalues. Details of the methods are described in Cliffe, Garratt & Spence (1993).

A range of Reynolds number was determined over which a single complex-conjugate pair of eigenvalues was observed to cross from the stable right-half to the unstable left-half complex plane, all other eigenvalues being stable. The location of the Hopf bifurcation point was then computed as a regular solution of the extended system of Griewank & Reddien (1983). A mixed finite-element discretization of the time-dependent version of (3) and (4) results in a $(k+l)$-dimensional vector equation of the form

$$\boldsymbol{B} \frac{\mathrm{d}\boldsymbol{x}}{\mathrm{d}t} + \boldsymbol{f}(\boldsymbol{x}; R) = \boldsymbol{0}, \tag{17}$$

where $\boldsymbol{x} \in \mathbb{R}^{k+l}$ is the vector of nodal velocity and pressure freedoms, $\boldsymbol{f}$: $\mathbb{R}^{k+l} \to \mathbb{R}^{k+l}$ is a nonlinear vector-valued function and $\boldsymbol{B}$ is a $((k+l) \times (k+l))$ matrix. The location of the Hopf bifurcation point, for which the null eigenvalue is $\gamma = 0 + \mathrm{i}\omega$ and the null eigenvector is $\boldsymbol{a} + \mathrm{i}\boldsymbol{b}$, may be computed by solving

$$\begin{pmatrix} \boldsymbol{f}(\boldsymbol{x}; R) \\ \boldsymbol{f}_x(\boldsymbol{x}; R)\boldsymbol{a} - \omega \boldsymbol{B}\boldsymbol{b} \\ \boldsymbol{l}^T \boldsymbol{a} - 1 \\ \boldsymbol{f}_x(\boldsymbol{x}; R)\boldsymbol{b} + \omega \boldsymbol{B}\boldsymbol{a} \\ \boldsymbol{l}^T \boldsymbol{b} \end{pmatrix} = \boldsymbol{0}. \tag{18}$$

Here $\boldsymbol{f}_x$ is the Jacobian matrix $\partial \boldsymbol{f}/\partial \boldsymbol{x}$ and $\boldsymbol{l}$ is a vector with which to normalize the eigenvector components $\boldsymbol{a}$ and $\boldsymbol{b}$.

An initial guess to start the Newton iteration to solve the nonlinear system (18) was provided by the solution to the Navier–Stokes equations, the imaginary part of the single eigenvalue pair with negative real part and the corresponding (complex) eigenvector.

5. Properties of attached vortices

The computations to be described in this section concern the steady flows that arise at moderately small Reynolds numbers, with particular interest in the formation and properties of the steady vortices attached to the lee of the cylinder. All the calculations were carried out using Dirichlet velocity data on the downstream boundary CD (cf. figure 1) of exactly the same form as that specified on the inlet boundary. The no-slip condition was imposed at the sidewalls.

As the Reynolds number is increased from zero the flow develops a slight fore-and-aft asymmetry (with respect to the cylinder) until, at some critical Reynolds number, a pair of steady vortices appear at the rear of the cylinder. Such an abrupt change in topology of the observed flow field has many of the hallmarks of a bifurcation of the solution of the dynamical flow problem. However, that appears not to be the case, based on our numerical studies in which the eigenvalue structure was examined for the flow perturbed about the numerically computed solution at a given Reynolds number. This was done using an in-house code based on the Crouzeix–Raviart method (cf. §4) and using the ENTWIFE code. In the former case the sign of the determinant of the Jacobian associated with the perturbed problem was examined as a function of the Reynolds number and showed no evidence of there being a singular point in a range of Reynolds numbers spanning the critical value at which the vortices first appeared. This finding was also confirmed by the studies with ENTWIFE in which the most dangerous eigenvalue of the perturbed problem was determined, and again there was no evidence whatsoever of any eigenvalue crossing into the unstable half-plane. Therefore, it would appear that the formation of the attached vortices is not associated with a bifurcation of the solution of the dynamical problem. It does, however, seem as though the dramatic change in structure of the flow field when the vortices first appear has a simple explanation in terms of singularity theory. If we consider only the kinematical properties of the flow it follows, for steady flows in two dimensions, that the stream function ψ is a Hamiltonian for the system $\dot{x} = \psi_y$ and $\dot{y} = -\psi_x$, and the formation of the vortices would appear to be associated with a critical point of the dynamical system for ψ. Thus, on passing through this critical point, the two new separation points on the body correspond to (half) saddle points, the new stagnation point downstream of the cylinder corresponds to a saddle point and the eyes of the vortices correspond to two elliptic points of the system, indicating that the topological change of the flow field is a property only of the kinematics and is not associated with a critical point of the dynamical problem.

The computations to be described in this section of the paper were carried out using the code FIDAP. Several convergence tests on this code are reported in Pritchard *et al.* (1992) and some further studies of its efficacy have been carried out by Chen (1990). Most of the results to be described were made using the $P_2^+ - P_1$ method of Crouzeix–Raviart, but some comparisons and checks were also made using the Taylor–Hood element. It was found in the computations that great care was needed in constructing the mesh in order to obtain the desired accuracy for the calculations,

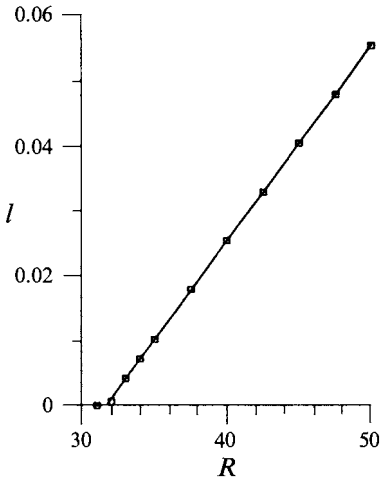

FIGURE 2. The length l of the recirculation zone as a function of the Reynolds number R for a cylinder of diameter $d = 0.2$.

particularly when trying to resolve the extent of the recirculating region behind the cylinder. So, for example, quite different kinds of triangulation strategies were needed with small cylinder diameters – $d = 0.1$ or 0.2 – than were needed with moderate ($d \sim 0.5$) or large ($d \sim 0.8$) cylinder diameters, details of which are given by Chen (1990).

The main characterization we have used for the recirculating region was the distance of its rear stagnation point from the cylinder, which distance we shall denote by l; we shall assume that l has been scaled relative to the cylinder diameter d. It is important to choose the length L of the domain and the placement of the cylinder in the domain such that neither the upstream nor the downstream computational boundaries influence the value of l to a noticeable extent. Preliminary investigations indicated that the value of l was less sensitive to the proximity of the upstream boundary than to the downstream boundary. A good balance seemed to be achieved with $L_1 = \frac{1}{3}L$, and we have used this apportionment throughout the current set of experiments. Accordingly, it was found in a series of experiments at $R = 80$ and with $d = 0.5$ that the length of the recirculating region was independent (to four decimal places) of the domain length L for values of L exceeding 7.5. The results to be described below, made at much smaller values of R, used the value $L = 6$.

In all of our numerical experiments it was found, to a very good approximation, that l increased nearly linearly with R, at least for values of l up to 0.2. Indeed, noticeable deviations from such a linear variation were always found to be associated with insufficiently accurate calculations. This was particularly so at very small values of l when an inordinately large number of mesh points was needed immediately behind the cylinder to resolve properly the details of the recirculating zone. An example, typical of all our numerical experiments, of the computed variation of l, for a cylinder of diameter $d = 0.2$, is shown in figure 2. The straight line shown in this graph is a linear least-squares regression fit of the data points for $l > 0$, and it is seen how closely they conform to the linear growth rate. Figure 2 shows that the smallest non-zero value of l lay slightly below the regression curve, and we believe, on the basis of our many other numerical experiments at different values of d, that a yet more accurate calculation would have moved the point close to the regression line. Note that the computation made at $R \approx 30.0$ gave no evidence of a recirculating region, further suggesting that the

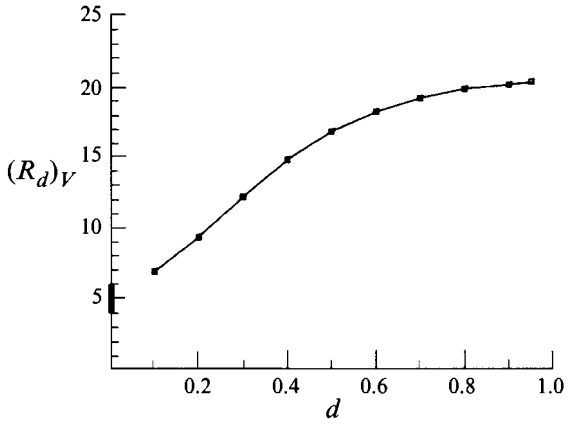

FIGURE 3. The critical Reynolds number $(R_d)_V$ at which the recirculation zone was established as a function of the cylinder diameter d. The heavy line between 4 and 6 on the ordinate indicates the range of experimental estimates for the critical Reynolds number in unbounded flows.

d	R_V	$(R_d)_V$	β
0.10	46.1	6.9	0.000966
0.20	31.6	9.3	0.00301
0.30	28.1	12.2	0.00484
0.40	26.1	14.8	0.00644
0.50	24.3	16.8	0.00776
0.60	23.0	18.2	0.00931
0.70	21.7	19.1	0.0107
0.80	21.0	19.8	0.0119
0.90	20.4	20.1	0.0130
0.95	20.4	20.3	0.0138

TABLE 1. The critical Reynolds numbers R_V and $(R_d)_V$ for the formation of the steady recirculation zone behind the cylinder. The quantity β denotes the (linear) rate of change of l with R.

intercept of the linear regression with the R-axis should have given a fairly accurate estimate of the critical value of R, which we shall denote by R_V, for the incipience of the vortices.

A summary of the main experimental results is given in table 1. In this table we have quoted the critical Reynolds number based on the separation between the walls and also the critical value of R_d based on the diameter of the cylinder. Also shown in the table is our estimate of the rate of growth of the vortex region with R, at least for l not too large. A graph of $(R_d)_V$ as a function of the cylinder diameter is given in figure 3, from which it is seen that the numerical estimates for the critical Reynolds number are apparently not far out of line with the experimental estimates obtained using very small values of d (i.e. in what are essentially unbounded domains).

6. Some periodic solutions

As R was increased in our numerical experiments it was found that the steady flows of the kind described in §5 could lose stability to a time-periodic flow. We shall consider some of the properties of such flows in this section and then, in §7, we shall

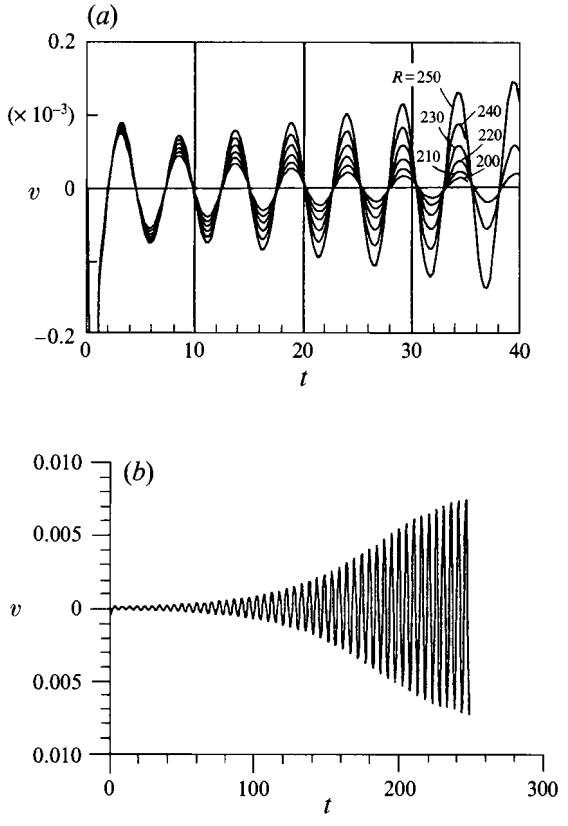

FIGURE 4. The velocity v computed at $x = (0.1148, 0)$ as a function of time, for a cylinder with $d = 0.2$. (*a*) Early phases in the development of v shown for a variety of Reynolds numbers. (*b*) Longer-term evolution of v at $R = 250$.

describe the results of sensitivity (bifurcation) studies relating closely to the present set of computations.

The numerical solutions to be described were all obtained on a flow domain of length $L = 9$, with $L_1 = 3$ (though it should be noted that confirmation of the general outcome of our experiments was obtained on longer domains). The boundary conditions used for the calculations were of Dirichlet type on both the inlet and outlet boundaries, with the velocity field being prescribed as $(\frac{1}{4} - y^2, 0)$. Thus the Reynolds number for the flow is $R = 1/(6\nu)$. In an attempt to locate new flows, either steady or unsteady, that would break the symmetrical structure in y enjoyed by the flows at small R, the following experiment was carried out. At a specified Reynolds number a computation was made of the (possibly unstable) steady, y-symmetric flow, the velocity and pressure fields of which were used as initial conditions for the following time-dependent computations: during the very early stages of the calculations, a small controlled perturbation was introduced to the flow via a perturbation of the boundary data, achieved by rotating the cylinder about its axis for a short period of time and then bringing it back to rest. Specifically, the boundary conditions at the surface of the cylinder were those of a uniform rotation for which the surface velocity V took the form $V = 10^{-3} \sin \pi t$, for $0 \leqslant t \leqslant 1$, and $V = 0$ thereafter. (We also experimented with other kinds of perturbations, which led to similar outcomes to those to be described, but a simple rotation of the cylinder was the most effective, introducing non-

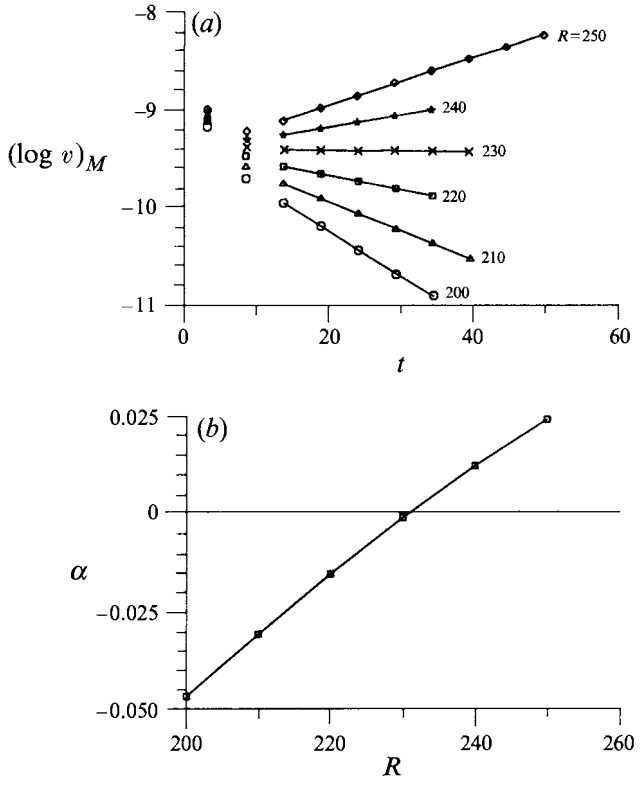

FIGURE 5. (*a*) Estimates of the initial growth rates (α) of the local maxima of $\log v$ (denoted by $(\log v)_M$ at a variety of Reynolds numbers, for a cylinder with $d = 0.2$. The straight lines are least-squares interpolations of the relevant data points. (*b*) The growth rates α plotted as a function of R.

symmetrical disturbances to the flow that would immediately affect the wake region.) The computations were carried out using the so-called Taylor–Hood element (cf. §4) for the spatial discretization and the Crank–Nicolson method was used for time stepping. The time step was fixed at 0.1 for $0 \leqslant t \leqslant 1$ and was set at values between 0.20 and 0.25 for larger times.

Numerical experiments have been carried out using cylinders of diameter $d = 0.2, 0.5$ and 0.7. The phenomena observed in each case bore close similarities, so we shall here describe in detail only the results for the case $d = 0.2$. The meshes used for these computations had approximately 10 000 degrees of freedom. Shown in figure 4(*a*) are temporal traces, found at a variety of Reynolds numbers, of the vertical velocity v at the point $\boldsymbol{x} = (0.1148, 0)$, on the axis immediately behind the cylinder. It is seen that, initially, v suffered a rather violent disturbance but, for t in excess of about 5, was nicely ordered with respect to t. An example of a longer temporal integration at $R = 250$ is shown in figure 4(*b*), the results of which suggest that the flow would have eventually settled down to a time-periodic motion.

Restricting attention to the smaller values of t for figure 4(*a*), it is seen that, at the smaller values of R, the velocity component v decayed towards zero whereas, at the larger values of R, it increased. The growth or decay of these disturbances were found to be nearly exponential in time, with growth rate α, say, as indicated by the plot shown in figure 5(*a*) of the local maxima of $\log v$ as a function of t. (The local maxima were determined from the discrete values of v by an interpolation procedure.) Here the lines

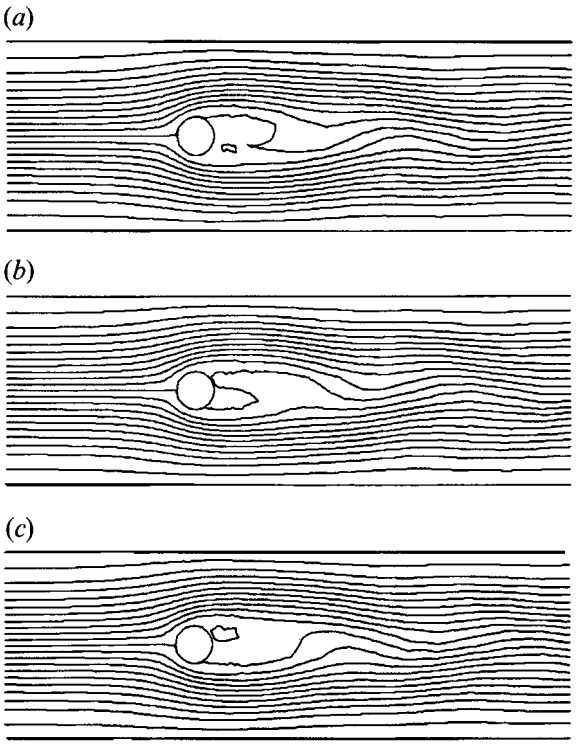

FIGURE 6. Streamline patterns at three different phases of a cycle of the relatively mature flow computed at $R = 250$ at a blockage ratio $d = 0.2$. Shown here is the portion of the computational domain such that $-1.0 \leqslant x \leqslant 2.0$. (*a*) Time $t = t_0 \approx 220$; (*b*) $t = t_0 + 1.7$; (*c*) $t = t_0 + 3.4$. Approximate period of cycle was 5.15.

joining the various data points are least-squares regression fits of the relevant data, and it is seen that they did indeed conform closely to a linear variation, once the initial hiatus produced by the rotation of the cylinder had subsided. The actual values of α thus obtained are indicated in figure 5(*b*). The data suggest that, for R less than approximately 231, the initial disturbance eventually decayed away and the original flow was re-attained, but for larger R the disturbances grew, giving rise to a new unsteady flow. We shall see in §7 that the present findings are in close agreement with the results of a numerical bifurcation study of the flow.

Streamline patterns of computed flows at three different phases of a cycle are shown in figure 6, indicating the oscillatory nature of the recirculating flow immediately to the rear of the cylinder. Some waviness of the streamline pattern downstream from the cylinder is evident, resulting from the detachment of a vortex blob, but it is also seen how the presence of the sidewalls eventually dominates the downstream properties of the flow field. Note that, for figure 6, the computational domain extended in the downstream direction to $x = 6$. The flow patterns shown here are slightly unusual in that they depict an asymmetric unsteady motion arising from the solution of a flow problem posed with steady symmetric Dirichlet data everywhere on the boundary of the flow domain.

Although the motions shown in figure 4 are not strictly periodic, the time between zero crossings of the vertical velocity field was found to be remarkably constant from cycle to cycle. Let this time interval be denoted by T. For a cylinder of diameter $d = 0.2$ the period T was estimated to be 5.15 for $R = 240$ and 250, leading to a Strouhal

number d/TU_d of approximately 0.17, to be compared with the experimental value of 0.15 found for flows in unbounded domains. For a blockage ratio $d = 0.5$ the Strouhal number for unsteady solutions slightly in excess of the critical Reynolds number was found to be approximately 0.36. For $d = 0.7$ it was found to be approximately 0.60.

7. Numerical bifurcation studies

Experiments were carried out to determine numerically the mechanism by which the small-Reynolds-number solution loses stability. These experiments were made using the sensitivity-analysis facility embodied in the code ENTWIFE, as described in §4. The numerical studies undertaken here were closely related to those described above in §6, The only difference being in the conditions imposed on the outflow boundary (CD of figure 1). For the computations described in §6, Dirichlet data were imposed on the outflow boundary, and here we have used the natural boundary conditions associated with the finite-element method we have employed (cf. the discussion in §4). (Attempts were made to carry out the bifurcation analysis using Dirichlet data, but these proved to be unsuccessful.) It should, however, be noted that, if the domain was chosen to be sufficiently long, the velocity profile recovered on the outlet boundary, resulting from the imposition of the natural boundary conditions, conformed closely with the Dirichlet conditions used in §6, and in that sense the two computations are closely related. One general point of agreement between the experiments of §6 and the present eigenvalue calculations is the feature that, in all cases, the bifurcation of the primary solution was to a Hopf flow, breaking both the symmetry and the time independence of the solution.

Eigenvalue analyses have been carried out with cylinders whose diameters ranged between 0.1 and 0.7. A typical mesh, on a domain of length $L = 10.5$, with $L_1 = 3$, is shown in figure 7 for a cylinder with $d = 0.4$. (Note that the finite-element method used for these calculations was based on a quadrilateralization of the domain.) Near the cylinder there is a radial gradation of the mesh, and away from the cylinder the mesh is also graded in both the upstream and downstream directions. The discrete approximation associated with such a mesh, which had approximately 13000 degrees of freedom for the velocity and pressure fields, was near the upper limit of the size of calculation possible on our machines. We believe that the eigenvalues presented below are within 1 % of the fully converged values, which estimate was arrived at on the basis of a large number of calculations made on domains of differing length, on different mesh grading strategies near the cylinder, and on a single much larger calculation.

The main results of our calculations are summarized in table 2. The estimates of the critical Reynolds number obtained from the eigenvalue calculations are given in the third column of the table and can be compared with the values obtained from the numerical experiments described in §6. The agreement between the two calculations is well within the experimental errors associated with the computations and, in particular, an extrapolation of the results from coarse to finer meshes suggests that the critical Reynolds numbers on yet more refined meshes would be slightly below the values cited in column 3 of the table. Shown in the fourth column of the table, and plotted below in figure 9 as a function of d, are the critical values of the Reynolds numbers when based on the diameter of the cylinder. Given in the fifth column are Strouhal numbers based on the imaginary part of the eigenvalue at bifurcation, the Strouhal number being defined as $St = d/TU_d$, where T is the period associated with the Hopf bifurcation. As discussed above, the loss of stability of the primay flow, as revealed by our calculations, occurs at a symmetry-breaking Hopf bifurcation, the structure of

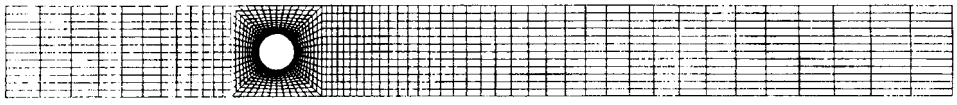

FIGURE 7. An example of the kind of mesh used for the eigenvalue calculations. Here $L = 10.5$, $L_1 = 3.0$, $d = 0.4$. This mesh had 13056 degrees of freedom associated with it.

(*a*)

(*b*)

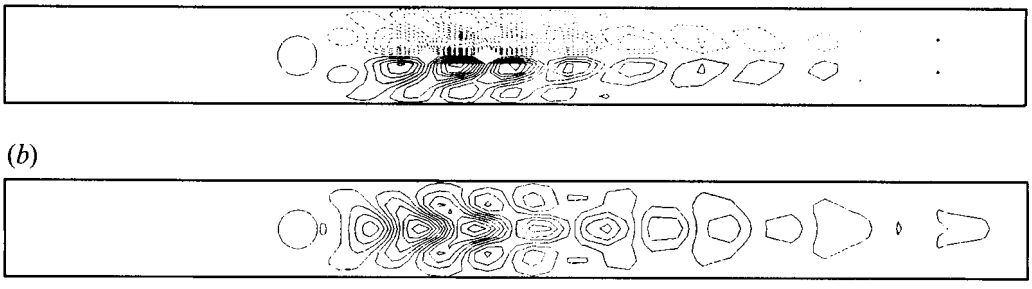

FIGURE 8. The components of the real part of the null-eigenvector associated with the bifurcation calculation. (*a*) The u-component (the dashed contours are the negative of the continuous ones); (*b*) the v-component. Here $L = 10.5$; $L_1 = 3.0$; $d = 0.4$.

d	R_A^*	R_B^*	R_d^*	St
0.10	—	345	51.6	0.122
0.15	—	263	58.8	0.137
0.20	231	233	69.0	0.158
0.30	—	211	92.0	0.215
0.40	—	194	110.1	0.286
0.50	166	166	114.2	0.369
0.60	—	131	103.6	0.463
0.70	105	106	92.9	0.567

TABLE 2. Estimates of the critical Reynolds numbers for the loss of stability of the primary solution for flow past a cylinder, for various values of the cylinder diameter, d. The column headed R_A^* gives estimates based on the calculations described in §6 and that headed R_B^* is based on the eigenvalue calculations; the column headed R_d^* is the critical Reynolds number based on the cylinder diameter, as computed from the eigenvalue calculations. The column headed St gives the Strouhal number at bifurcation.

which can be discerned from the plots shown in figure 8 of the u- and v-components of the real part of the null eigenvector (the complex eigenvector associated with the eigenvalue having zero real part at the bifurcation point). The u-velocity component of the low-Reynolds-number 'symmetric' flow has reflectional symmetry about the line $y = 0$ and the v-velocity component is antisymmetric. The velocity components of the null symmetry-breaking eigenvector must have the opposite symmetries and indeed it can be seen that the u-component of the real part of the eigenvector is antisymmetric about the centreline and the v-component is symmetric. It is also seen that the magnitude of the eigenvectors decayed rapidly downstream of the cylinder, reinforcing the claim that the results presented here should be nearly independent of the downstream extent of the domain. The u- and v-velocity components of the imaginary part of the eigenvector were similar.

Extensive calculations have also been made to investigate the so-called 'free-stream' case, namely the problem considered by Jackson (1987) as described in §1, meant to

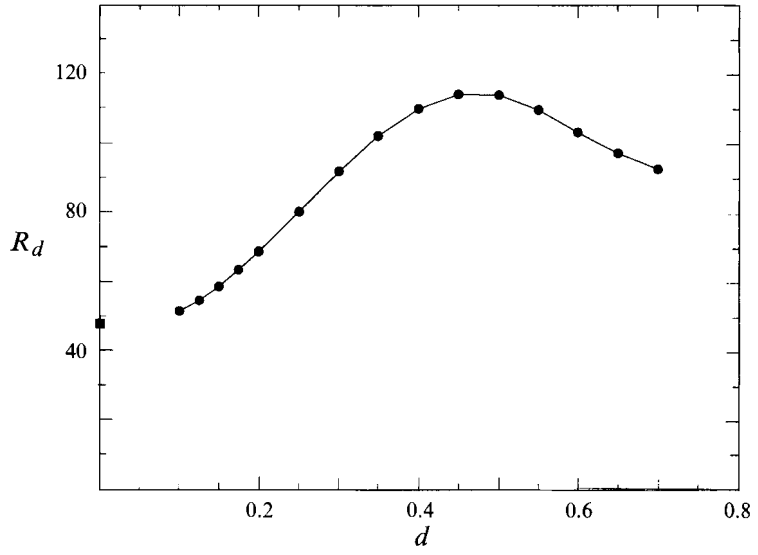

FIGURE 9. The results of the eigenvalue calculations of the critical Reynolds number, based on the diameter of the cylinder, as a function of blockage ratio d. The point represented by the black square denotes the value obtained from the 'free-stream' case, meant to simulate an unbounded domain.

simulate flow in an unbounded domain. Our experiments included extensions to the domain in both the downstream and lateral directions, as well as experimenting with the gradation and size of the mesh, but the boundary conditions were kept the same as those employed by Jackson. By and large, the results of the present calculations are in fairly close agreement with those given by Jackson. Thus, for example, we have estimated the critical Reynolds number for the free-stream case to be 47.9 with a corresponding Strouhal number of 0.138, to be compared with Jackson's respective estimates of 46.2 and 0.138. Shown in figure 9 is a plot of the computed critical Reynolds numbers (based on the cylinder diameter), as a function of d, and also included in the figure is the free-stream value, to which we have chosen to assign the value $d = 0$.

8. Concluding remarks

It is apparent from the above discussion that the current evidence concerning the nature of the bifurcation of the steady flow past a cylinder or sphere with increasing Reynolds number is in a somewhat confused state. For flow past a cylinder, the experiments are fairly uniform in suggesting that an unsteadiness appears in the wake at a Reynolds number of 35 or thereabouts, whereas the numerical experiments of Jackson (1987) indicate a loss of stability to a Hopf bifurcation at a Reynolds number of approximately 46. For flow past a sphere there is experimental evidence for the bifurcation to be to a time-periodic flow (Taneda 1956*b*) and there is also evidence for the bifurcation to be to a symmetry-breaking steady flow (Nakamura 1976; Wu & Faeth 1993). Computationally it has been suggested, on the one hand, that the bifurcation is to a symmetry-breaking Hopf flow and, on the other, that it is to symmetry-breaking steady flow.

It is our view that the main difficulties associated with these problems arise, both experimentally and computationally, through the desire to approximate flows on

unbounded domains and that, if the flow be confined between parallel planes or to a circular pipe, the problem becomes much more manageable. The reason for this is that the asymptotic structure of the flow, both upstream and downstream of the body, is determined by the influence of the confining walls, so that the flow on the apparently unbounded domain of the pipe can be closely approximated by a Dirichlet problem for flow on a bounded domain. The confinement of the flow between parallel planes, or to a circular pipe, does not appear to change the physical structure of the flow or its bifurcation properties in a dramatic manner, especially if the ratio of the diameter of the cylinder to the separation between the walls is fairly small.

Thus, in the present paper, it is suggested on the basis of two entirely different kinds of numerical experiments, that the steady flow past a cylinder confined between parallel planes loses stability, with increasing Reynolds number, through a symmetry-breaking Hopf bifurcation, with the value of the critical Reynolds number at bifurcation being dependent on the diameter of the cylinder relative to the separation of the walls.

The same techniques may be applied to the case of flow past a sphere in a circular pipe and, using such, Tavener (1994) has determined the bifurcation to be to an asymmetric steady flow, breaking the O(2)-symmetry of the original flow, to be contrasted with the bifurcation in the two-dimensional case to an asymmetric, unsteady Hopf flow.

REFERENCES

AMICK, C. J. 1977 Steady solutions of the Navier–Stokes equations in unbounded channels and pipes. *Ann. Scuola Norm. Sup. Pisa IV* **4**, 473–513.

AMICK, C. J. 1978 Properties of steady Navier–Stokes solutions for certain unbounded channels and pipes. *Nonlinear Anal.* **2**, 689–720.

AMICK, C. J. & FRAENKEL, L. E. 1980 Steady solutions of the Navier–Stokes equations representing plane flow in channels of various types. *Acta Mathematica* **144**, 83–152.

BATCHELOR, G. K. 1967 *An Introduction to Fluid Dynamics*. Cambridge University Press.

BERCOVIER, M. & ENGELMAN, M. 1979 A finite element method for the numerical solution of viscous incompressible flows. *J. Comput. Phys.* **30**, 181–201.

CHEN, J.-H. 1990 A numerical study of flow past a cylindrical body. PhD dissertation, Penn State University.

CLIFFE, K. A., GARRATT, T. J. & SPENCE, A. 1993 A modified Cayley transform for the discretized Navier–Stokes equations. In *Proc. ISNA '92, Applications of Mathematics*, vol. 38, pp. 281–288.

COUTANCEAU, M. & BOUARD, R. 1977*a* Experimental determination of the main features of viscous flow in the wake of a circular cylinder in uniform translation. Part 1. Steady flow. *J. Fluid Mech.* **79**, 231–256.

COUTANCEAU, M. & BOUARD, R. 1977*b* Experimental determination of the main features of viscous flow in the wake of a circular cylinder in uniform translation. Part 2. Unsteady flow. *J. Fluid Mech.* **79**, 257–272.

CROUZEIX, M. & RAVIART, P.-A. 1973 Conforming and non-conforming finite element methods for solving the stationary Stokes equations. *RAIRO* **R-3**, 33–76.

ENGELMAN, M. 1982 FIDAP – A fluid dynamics analysis package. *Adv. Engng Software* **4**, 163–166.

FEARN, R. M., MULLIN, T. & CLIFFE, K. A. 1990 Nonlinear flow phenomena in a sudden symmetric expansion. *J. Fluid Mech.* **211**, 595–608.

GERRARD, J. H. 1978 The wakes of cylindrical bluff bodies at low Reynolds number. *Phil. Trans. R. Soc. Lond.* A **288**, 351–382.

GRIEWANK, A. & REDDIEN, G. 1983 The calculation of Hopf points by a direct method. *IMA J. Numer. Anal.* **3**, 295–304.

GUNZBURGER, M. D. 1989 *Finite Element Methods for Viscous Incompressible Flows*. Academic.

JACKSON, C. P. 1987 A finite-element study of the onset of vortex shedding in flow past variously shaped bodies. *J. Fluid Mech.* **182**, 23–45.

KIM, I. & PEARLSTEIN, A. J. 1990 Stability of flow past a sphere. *J. Fluid Mech.* **211**, 73–93.

LODGE, A. S., PRITCHARD, W. G. & SCOTT, L. R. 1991 The hole-pressure problem. *IMA J. Appl. Maths.* **46**, 39–66.

NAKAMURA, I. 1976 Steady wake behind a sphere. *Phys. Fluids* **19**, 5–8.

NATARAJAN, R. & ACRIVOS, A. 1993 The instability of the steady flow past spheres and disks. *J. Fluid Mech.* **254**, 323–344.

NISHIOKA, M. & SATO, H. 1974 Measurements of velocity distributions in the wake of a circular cylinder at low Reynolds numbers. *J. Fluid Mech.* **65**, 97–112.

PRITCHARD, W. G. 1983 Some viscous-dominated flows. In *Trends and Applications of Pure Mathematics to Mechanics* (ed. P. G. Ciarlet & M. Rousseau), pp. 305–332. Springer.

PRITCHARD, W. G., SCOTT, L. R. & TAVENER, S. J. 1992 Numerical and asymptotic methods for certain viscous free-surface flows. *Phil. Trans. R. Soc. Lond.* A **340**, 1–45.

PROVANSAL, M., MATHIS, C. & BOYER, L. 1987 Bénard–von Kármán instability: transient and forced regimes. *J. Fluid Mech.* **182**, 1–22.

TANEDA, S. 1956*a* Experimental investigation of the wakes behind cylinders and plates at low Reynolds numbers. *J. Phys. Soc. Japan* **11**, 302–307.

TANEDA, S. 1956*b* Experimental investigation of the wake behind a sphere at low Reynolds numbers. *J. Phys. Soc. Japan* **11**, 1104–1108.

TAVENER, S. J. 1994 Bifurcation of the O(2)-symmetric flow past a sphere in a pipe. To appear in Phys. Fluids.

TAYLOR, C. & HOOD, P. 1973 A numerical solution of the Navier–Stokes equations using the finite element technique. *Comput. Fluids* **1**, 73–100.

TRITTON, D. J. 1959 Experiments on the flow past a circular cylinder at low Reynolds numbers. *J. Fluid Mech.* **6**, 547–567.

WINTERS, K. H. 1985 ENTWIFE user manual (release 1). *Harwell Rep.* AERE-R 11577.

WU, J. S. & FAETH, G. M. 1993 Sphere wakes in still surroundings at intermediate Reynolds numbers. *AIAA J.* **31**, 1448–1455.